A Low-Cost, Portable and Robust Calibration Method for Industrial Robot

A Low-Cost, Portable and Robust Calibration Method for Industrial Robot*

Yuxuan Zhang
School of Engineering and Physical Sciences
Heriot-Watt University
Edinburgh, United Kingdom
yz2115@hw.ac.uk

Lijuan Luo
School of Computing, Engineering & the Build Environment
Edinburgh Napier University
Edinburgh, United Kingdom
L.Luo@napier.ac.uk
0000-0003-4199-493X

Kun Qian
School of Engineering
University of Manchester,
Manchester, United Kingdom
kun.qian@manchester.ac.uk
0000-0002-8719-1537

Xianwen Kong[1]
School of Engineering and Physical Sciences
Heriot-Watt University
Edinburgh, Kingdom
x.kong@hw.ac.uk
0000-0001-6747-7768

***Abstract*—Industrial robot calibration is crucial for high-precision operations. This paper introduces a low-cost, portable calibration method using a fixture with three digital indicators and an adaptable artifact, reducing reliance on expensive tools like laser trackers and Coordinate Measuring Machines (CMMs). By integrating the least squares (LS) and Levenberg-Marquardt (LM) algorithms with the Extended Kalman Filter (EKF), the system can significantly enhance calibration accuracy and efficiency. Experimental results show that an increasing number of planes (from 4 to 7) used on the artifact can improve the calibration accuracy by 10%, and a reduction of end-effector pose measurements (from 175 to 91 poses provided by the artifact) can increase the calibration efficiency by 47.7% with a minimal accuracy loss of 2.03%. Results illustrate the effectiveness of the proposed portable system in improving the accuracy of robot kinematics, demonstrating its great potential in robot-assisted manufacturing and assembly.**

Keywords—Robot Calibration, Kinematics, Optimization, Robotic Manufacturing.

I. INTRODUCTION

Robotic manipulators have been extensively used in manufacturing tasks such as material handling, welding, and painting tasks involved high levels of repeatability[1][2]. However, in this type of operation, performance expectations of accuracy are low [2]. Nevertheless, with the development of industrial robots in fields like aviation and medicine, the performance expectations of accuracy have greatly increased[2]. To enhance accuracy, both geometric and non-geometric factors need to be considered[3]. Geometric error includes assembly error, manufacturing error, connecting rod parameter error, and joint angle parameter error, while non-geometric errors include joint flexibility, friction, joint clearance and so on[4].

Under this circumstance, one important technology, robot calibration, aims to eliminate errors including both geometric and non-geometric ones and improve positioning accuracy [4] . The basic idea of robot kinematics calibration involves describing the structure and motion characteristics of the robot through the Denavit-Hartenberg (D-H) model, then measuring the Tool Centre Point (TCP) position, and finally using an algorithm to make the TCP position wirelessly close to the calibration position. Numerous scholars have studied methods for measuring the TCP position and optimizing algorithms. For instance, Wang et al. [5] introduces a low-cost, open-loop, and high-accuracy method for calibrating industrial robots, utilizing a single Position Sensitive Device (PSD). This method is based on the analysis of a monocular vision six-degree-of-freedom spatial position estimation technique and introduces a "three-point" spatial position measurement model tailored for robot calibration. However, this method is not suitable for environments with outdoor and dusty conditions. To address this problem, a robust method should be proposed to assist the industry in solving robot calibration challenges. The method by Icli et al. [6] employs a closed-loop system featuring a fixture with three digital indicators and an artifact that includes four 1-inch datum balls mounted on stems. A Coordinate Measuring Machine (CMM) is used to measure their relative positions. However, the improvement in accuracy and efficiency needs to be considered. Some scholars [7] use algorithms to improve robot calibration accuracy. Nadeau et al. [8] utilized a laser tracker measurement model combined with the LS technique to enhance calibration accuracy. However, their method does not address the issue of singularity.

Therefore, in this study, a low-cost, robust and portable approach is proposed to improve robot calibration accuracy and efficacy. It integrates LS algorithm with EKF and also LM with EKF for resolving the singularity issue. An xArm 6 six- axis serial robot as shown in Fig. 1, equipped with a high- precision connector, is used to touch the barball. The barball position is confirmed by a Coordinate Measuring Machine (CMM). After measurement, an optimization method is applied to identify and compensate for errors to enhance robot calibration accuracy. Furthermore, the study proposes a selective procedure to reduce the number of measurement points, thus improving measurement efficiency.

* This work is partially supported by the Engineering and Physical Sciences Research Council [EP/T024844/1]
[1] Corresponding author

II. METHODOLOGY

In order to identify the geometric errors of each joint, this study will apply a modified DH (MDH) model [3] and Jacobian matrix to establish the relationship between each link. Forward kinematics will be utilized to determine the nominal position, including the geometric error of the end-effector. A new measurement approach, employing three 45° planes, will be used to ascertain the real position of the end-effector. Error compensation will be achieved using the LS algorithm, LM algorithm, EKF algorithm, and combination algorithms as EKF with LM algorithm and EKF with LS algorithm.

The experimental setup includes an xArm 6 robot, metal connectors, TriCal, three digital indicators, a 1.5-inch ball, a barball, and 3D printed artifact. Joint angle data is collected through the xArm 6 robot's API. Matlab is utilized to execute the forward kinematics computations and optimization algorithms. The method for data measurement involves manually positioning the robot near the target location, followed by employing the robot's API to execute precise displacements, shown as Fig. 1.

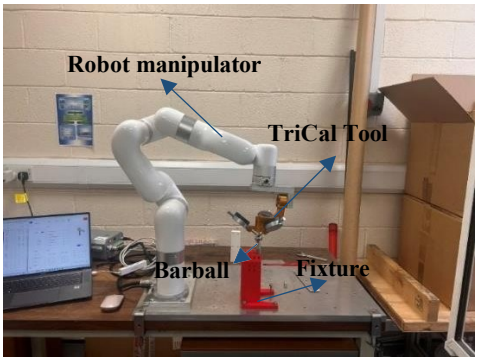

Fig. 1. Robot calibration experiment.

Robot calibration has four steps: 1. Robot kinematic modelling; 2. End-effector position measurement; 3. Robot kinematic identification; 4. Kinematic errors compensation.

A. Robot kinematic modelling

D-H model and MDH model are widely used in robot calibration. The difference between D-H model and MDH model is that they have different fixed coordinate systems for the joints. The MDH model is applied in this paper to solve the compatibility problem with 3D drawing software, and it was also effective in inverse kinematic [4], as shown in table 1. The MDH model can be described as

$$ {}^{i-1}_{i}T = R_X(\alpha_{i-1}) \times D_X(\alpha_{i-1}) \times R_Z(\theta_i) \times D_Z(d_i) $$

$$ = \begin{bmatrix} cos\theta_i & -sin\theta_i & 0 & a_{i-1} \\ sin\theta_i cos\alpha_{i-1} & cos\theta_i cos\alpha_{i-1} & -sin\alpha_{i-1} & sin\alpha_{i-1} d_i \\ sin\theta_i sin\alpha_{i-1} & cos\theta_i cos\alpha_{i-1} & cos\alpha_i & cos\alpha_{i-1} d_i \\ 0 & 0 & 0 & 1 \end{bmatrix} \quad (1) $$

where l_n is the distance from z_n to z_{n+1} and the measured along x_n, α_n is the angle form z_n to z_{n+1} and the measured along x_n . d_n is the distance from x_n to x_{n-1} and the measured along z_n, and θ_n is the angle from x_n to x_{n-1} and the measured along z_n. The formula form link (*i*) to link (*i*-1) can be referred to [4] and [9]. The kinematic equation of a robot can then be set up as

$$ T_0^6 = T_0^1 T_1^2 T_2^3 T_3^4 T_4^5 T_5^6 \quad (2) $$

The error in transformation matrix is generated by the deviation in MDH parameter for each link, and can be expressed as follows:

$$ T_0^6 + dT_0^6 = (T_0^1 + dT_0^1)(T_1^2 + dT_1^2) \quad (3) $$
$$ (T_2^3 + dT_2^3)(T_3^4 + dT_3^4)(T_4^5 + dT_4^5)(T_5^6 + dT_5^6) $$

The linear combination of deviations in D-H parameters is approximately equal to the error in the transformation matrix of the connecting link. Thus, we have

$$ dT_{i-1}^i = \frac{\partial T_{i-1}^i}{\partial \alpha_{i-1}} d\alpha_{i-1} + \frac{\partial T_{i-1}^i}{\partial a_{i-1}} da_{i-1} + \frac{\partial T_{i-1}^i}{\partial d_i} dd_i + \frac{\partial T_{i-1}^i}{\partial \theta_i} d\theta_i \quad (4) $$

And Eq. (6) can be expanded as:

$$ dT_0^N = \sum_{i=1}^{n} (T_0^1 T_1^2 \dots T_{i-1}^i \delta T_{i-1}^i \dots T_{N-1}^N) \quad (5) $$

The linear relationship between the position error of the robot end-effector and the error in kinematic parameters is as follows:

$$ \Delta E = [J_a \quad J_d \quad J_\alpha \quad J_\theta] \begin{bmatrix} \Delta_a \\ \Delta_d \\ \Delta_\alpha \\ \Delta_\theta \end{bmatrix} = J\Delta\omega \quad (6) $$

where J represents the differential identification Jacobian matrix of the manipulator arm; $\Delta\omega$ is the robot kinematic parameters deviations and ΔE is the first three line of the last column of the matrix dT_0^6. Then the following function can be obtained as:

$$ \varepsilon = \frac{1}{n} \sum_{i=1}^{n} \frac{1}{2} (Y_i - \hat{Y}_i) \quad (7) $$

$$ Y_i = \sqrt{(x_i - x_0)^2 + (y_i - y_0)^2 + (z_i - z_0)^2} \quad (8) $$

$$ \hat{Y}_i = \sqrt{(\hat{x}_i - x_0)^2 + (\hat{y}_i - y_0)^2 + (\hat{z}_i - z_0)^2} \quad (9) $$

where Y is the measure length and $\hat{Y}$ is the nominal length. The position (x_0, y_0, z_0) is the point which is the position where the upper rear center point of the artifact is vertically mapped to the base plane.

TABLE I. KINEMATIC PARAMETERS OF XARM 6

i	α_{i-1}	a_{i-1}	d_i	θ_i
1	0	0	267	0
2	-pi/2	0	0	0
3	0	249.5	0	0
4	-pi/2	77.5	342.5	0
5	pi/2	0	0	0
6	-pi/2	76	97	0

B. End-effector position measurement

In the experimental, a 3D scanner was used to measure the position of the barball, nonreflective bolts are used to replace the barball, and geometric calculations were used to determine

the specific position. The total number of measurement points is 34 which contains two measurement positions, each measurement position consists of 5 measurement points on the horizontal plane and 2 measurement points on each of the other faces, the first four data are shown in table 2.

TABLE 2. THE FIRST FOUR DATA OF MEASURE POSITION

Number		x	y	z
1	A	295.3	-19.6	204.8
	B	492.2	-27.2	201.6
2	A	280	-4.6	204.7
	B	477.5	-12.6	200.8
3	A	280.1	-34.9	204.3
	B	477.2	-42.5	200
4	A	310.6	-4.6	204.1
	B	507.3	-12.7	200.8

Icli [6] introduced that using a 1.5-inch standard ball to set the digital indicators. Once the cue ball is positioned, each indicator should be adjusted to display 6.350 mm. When using a 1-inch ball, it should read 0, the focus of the indicator extension line is the centre of the ball. Given that the same TriCal is used in this experiment, the indicator will display 12.350 mm when the cue ball is placed, and 6 mm when the 1-inch ball indicator is used, the focus of the indicator extension line is the centre of the ball, as shown in Fig. 2.

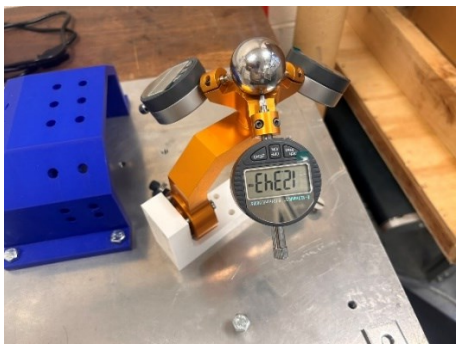

Fig. 2. Using TriCal to confirm the centre point of the barball

C. Robot kinematic identification

Robot kinematic identification aims to use optimization algorithms to identify errors in MDH models. The most widely used is the least square method [4]. Other algorithms such as LM algorithm, maximum-likelihood estimation (MLE), and Kalman filter (KF) algorithm have also been implemented to identify robot kinematic parameters. In this paper, LS, LM, LS with EKF, and LM with EKF algorithms were used to identify error parameters.

The LS algorithm and the LM algorithm are algorithms for finding the optimal solution. The EKF algorithm is an algorithm for eliminating nonlinear noise [4]. This article combines the EFK algorithm with the LS and LM algorithms respectively to improve the accuracy of robot calibration. Flowchart of robot calibration as shown in Fig. 3.

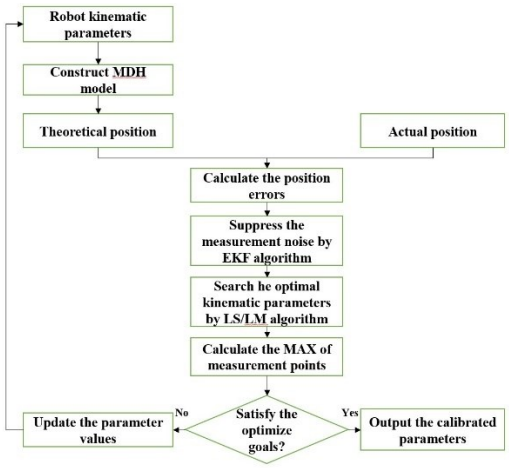

Fig. 3. Flowchart of robot calibration.

Finally, error parameters are added to the MDH model to achieve motion error compensation.

D. Data collection

In order to demonstrate the effectiveness of the experiment, three experimental methods were proposed. The selection of the barball's location is depicted in Fig. 4. These locations represent the positions on the artifact.

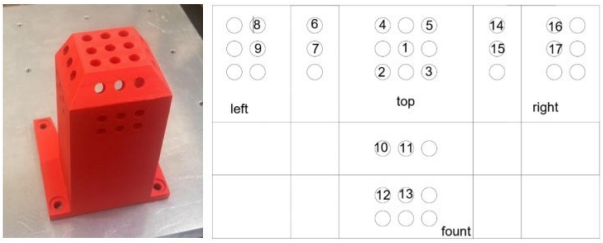

Fig. 4. Location selection of the barball.

The sampling points will be collected on the barball. Points directly above the ball and on 3 planes at 45°, 90°, and 135° will be selected, with 8 points in 8 directions on each 31 plane. For each ball, 25 points will be chosen. The TCP position of the measuring point on the ball is considered the centre of the ball. L is the distance between TCP and the point (x_0, y_0, z_0).

The name of the experiment, the description of the experiment and the number of measurement points used in the experiment are shown in Table 3. The first experiment discusses two distinct collection methods in the articles by [6], referred to as Experiment 1(a) and Experiment 1(b). This article proposes adding three directions, labeled as Experiment 1(c).

In the second experiment, given the increased number of measurement points in the first method, which may lead to potential unreliability, this experiment aims to balance the number of points. Specifically, Experiment 2(a) will be compared with Experiment 2(b), and Experiment 2(c) with Experiment 2(d).

The third experiment, Experiment 3(a), involves one point directly above, four points at 90° to represent upper points, four points at 45° as middle points, and the last four points at another 90° (or 270° from the original direction, for clarity) as lower points, totaling 9 points (note: the total mentioned as 91

seems to be a mistake based on the description). This method will be compared with Experiment 3(b) and Experiment 3(c).

TABLE 3. POSITION SELECTIONS. S: SURFACE AND L: LOCATION.

Name	Method name	Locations select	Number
Experiment 1			
(a)	1S3L	1, 2, and 3	75
(b)	4S4L	1, 9, 13, and 17	100
(c)	7S7L	1, 7, 9, 11, 13, 15, and 17	175
Experiment 2			
(a)	4S7L	1, 8, 9, 12, 13, 16, and 15	175
(b)	7S7L	1, 7, 9, 11, 13, 15, and 17	175
(c)	4S4L	1, 2, 3, and 4	100
(d)	1S4L	1, 9, 13, and 17	100
Experiment 3			
(a)	7S7L	1, 7, 9, 11, 13, 15, and 17	91
(b)	4S4L	1, 9, 13, and 17	100
(c)	7S7L	1, 7, 9, 11, 13, 15, and 17	175

E. Evaluation metrics

A The root mean square error (RMSE) and mean error (mean) were used as evaluation metrics to evaluate our approach shown as [10]:

$$\begin{cases} E_{RMSE} = \sqrt{\frac{1}{n}\sum_{i=1}^{n}\sqrt{(Y_i - \hat{Y}_i)^2}} \\ E_{Mean} = \frac{1}{n}\sum_{i=1}^{n}\sqrt{(Y_i - \hat{Y}_i)^2} \end{cases} \quad (10)$$

III. FINDINGS

Overall data performance as shown in Table 4. The performances of the LS algorithm, LS with EKF algorithm, LM algorithm, and LM with EKF algorithm are similar, with RMSE and mean values improved by 60%. Among them, LM with EKF performs better, followed by LS with EKF.

TABLE 4. OVER ALL DATA PERFORMANCE. (UNIT: MM)

	RMSE	MEAN
Original data	10.996	8.7
LS	4.5	3.5
LS with EKF	4.17	3.18
LM	4.23	3.17
LM with EKF	4.1	3.1

A. First Experiment

The first experiment aims to demonstrate that calibration accuracy is higher with seven surfaces than with four surfaces calibration method and the one surface three-point calibration method. In this initial experiment, the EKF with LM algorithm outperformed other algorithms, as shown in Table 5.

TABLE 5. PERFORMANCE OF LM WITH EKF (UNIT: MM)

	Training		Testing	
	RMSE	mean	RMSE	mean
Experiment 1(a)	1.74	1.04	6.21	4.26
Experiment 1(b)	4.3	3.27	5.4	4.16
Experiment 1(c)	4	3.14	4.64	2.61

In the three experimental training sets of Experiment 1, the performance of the EKF algorithm is similar to that in the original data, with an increased accuracy of 40%. In the test set, the EKF algorithm improves accuracy by 20%. Due to the small training dataset, the LS algorithm in Experiment 1(a), the RMSE and mean values are larger than those in Experiment 1(b), i.e., 1.78 mm and 1.68 mm. In Experiment 1(c), the training and test datasets of the LS algorithm closely match those of the other three algorithms, with only a 0.5mm difference in the RMSE and MEAN parameter values. In Experiment 1(a), the error is within 0.5mm of that produced by the LS with EKF, LM, and LM with EKF algorithms. Conversely, in Experiments 1(b) and 1(c), the error is 4-5 mm and 3-3.5 mm lower than those algorithms, respectively.

Since the data from the four algorithms are very close, the LM with EKF algorithm, which shows the best performance, is selected based on the mutual comparison across the three sub-experiments. Experiment 1(a) 41 performed best in the training set, showing a very significant improvement in accuracy with an increase of 90%, which is much higher than the 60-70% observed in Experiments 1(b) and 1(c). This is attributable to two factors: first, the dataset consisted of only 75 experimental data points; second, only one plane is selected for the experiment. In the test set, Experiment 1(c) performs best. This aligns with the expectation that as the experimental measurement positions and the amount of experimental data increase, the testing outcomes will improve.

B. Second Experiment

The objective of Experiment 2 is to demonstrate that maintaining the same number of measurement points while increasing the number of measurement surfaces can enhance measurement accuracy. Experiment 2 is divided into two parts. The first part, comprising sub-experiments experiment 2(a) and experiment 2(b), explores different plane configurations. The second part includes sub-experiments experiment 2(c) and experiment 2(d), where experiment 2(d) involves selecting four positions on the horizontal plane, and experiment 2(c) involves selecting one position on the horizontal plane and one on each of three vertical planes, with both sub-experiments totalling 100 measurements. The EKF algorithm performs similarly in the test set and does not show improvement, despite factors such as increasing measurement surface area and direction. In contrast, the accuracy improves as the measurement surface area increases.

In the Experiment 2(a) test set, the RMSE values for the algorithms range from 4.45 to 4.8. In the Experiment 2(b) test

set, the RMSE values for these algorithms range from 3.9 to 4.3, as shown in Fig. 5. The LS with EKF algorithm exhibits the smallest RMSE and mean values in both Experiment 2(a) and Experiment 2(b). Additionally, the RMSE and mean values in Experiment 2(b) are 0.52mm and 0.19mm lower, respectively, than those in Experiment 2(a).

In Experiment 2(c), the LS algorithm achieves the best results in terms of RMSE and mean values, shown as table 6. In Experiment 2(d), the LS with EKF algorithm shows the best optimization effect, with RMSE and mean values of 4.69mm and 3.76mm, respectively. The results of Experiment 2(c) are better than those of Experiment 2(d), which aligns with the expectation that increasing the measurement surface will improve accuracy, provided that the number of measurement points is maintained.

Fig. 5. Sub-experiment 1 test result

TABLE 6. SUB-EXPERIMENT 2 VALUES (UNIT: MM).

		Experiment 2(c)	Experiment 2(d)
Algorithm		LSEKF	LSEKF
Original data	RMSE	11.36	11.36
	mean	8.91	8.91
Testing	RMSE	4	4.69
	mean	3.26	3.76

C. *Third Experiment*

The final experiment will be conducted with two comparative tests. Comparative test one involves experiments 3(a) and 3(c), as shown in Fig. 6. Experiment 3(a) is similar to Experiment 3(c), but the number of points at each bat position is reduced by 12. However, it is necessary to ensure that there are measurement points in all eight directions of the bat. Comparative test two involves experiments 3(a) and 3(b). In Experiment 3(b), a measurement position is chosen on each of the horizontal plane and three vertical planes, similar to Experiment 1(b), but the test set is same as experiments 3(a).

Compared with Experiment 3(a), Experiment 3(c) demonstrates better performance, which aligns with the expected improvement due to increased measurement points and higher accuracy. In both Experiment 3(a) and Experiment 3(c), the LS with EKF algorithm performs best. The accuracy difference between Experiment 3(a) and Experiment 3(c) is only 0.16mm in RMSE and 0.19mm in mean, yet the number of measurement points in Experiment 3(a) is nearly half that of Experiment 3(c), which 45 signifies a significant improvement in measurement efficiency. In summary, Experiment 3(c) enhances efficiency by 47.70% while only reducing accuracy by 2.03%, relative to Experiment 3(a). Accuracy is calculated as the percentage derived from 1 minus the ratio of the sum of the Root Mean Square Error (RMSE) and the mean to the sum of the RMSE and mean values from the original data of Experiment 3(a). Efficiency is determined by the percentage of 1 minus the ratio of the number of measurement points utilized to 175.

To identify the optimal trade-off between accuracy reduction and efficiency improvement, an additional series of experiments was conducted as shown in Fig. 7. As illustrated in the accompanying table 7, the ideal balance point occurs at 91 measurement points, which 46 yields a 47.7% increase in efficiency and a marginal accuracy decrease of 2.03%.

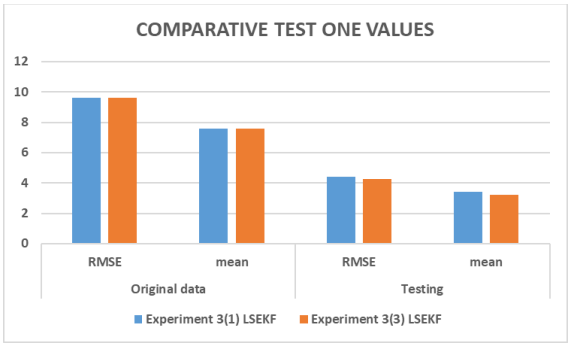

Fig. 6. Comparative test 3(a) and 3(c) values

TABLE 7. ADDITIONAL EXPERIMENT VALUES

Number	RMSE	MEAN	Increase efficiency	Reduce accuracy
175	4.27	3.23	0%	0%
168	4.35	3.37	3.90%	1.20%
161	4.38	3.36	7.90%	1.40%
154	4.38	3.37	11.90%	1.45%
133	4.51	3.53	23.80%	3.14%
112	4.51	3.46	35.70%	2.73%
98	4.47	3.45	43.70%	2.40%
91	4.43	3.42	47.70%	2.03%
84	4.45	3.45	51.70%	2.33%

Experiment 3(a) selects 9 fewer measurement points than Experiment 3(b), yet it demonstrates better performance with lower RMSE and mean. The best performing algorithm is the LS with EKF algorithm. In Experiment 3(a) values are lower than those in Experiment 3(b). This result further underscores the importance of increasing the measurement surface.

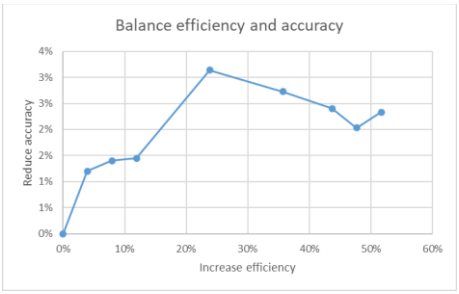

Fig. 7. Trade-off between accuracy and efficiency of the system

IV. Discussion

The total cost of the calibration device is less than $2,500, which is significantly lower than that of methods such as the novel 6D measurement system ($13,000), coordinate measuring machines, and laser trackers [6]. Moreover, this cost is $500 less than the method proposed by [6]. Compared with open-loop measurement methods such as laser trackers and cameras, the robustness of the measurement method used in this study is not affected by environmental factors such as temperature, humidity, and dust [10], as shown in table 8.

TABLE 8. COMPARISON OF THREE METHODS

Comparison	Proposed method(mm)	Icli method [6] (mm)	Laser Tracker(mm)
Accuracy	0.84	1	0.60
Efficiency	0.91	1	0.33
Cost	USD 2500	USD 5000	USD 100,000
Robust	Yes	Yes	No
Portable	Yes	Yes	No

Furthermore, in contrast to the draw-wire sensor method proposed by [10], this method offers greater flexibility and requires less installation time for the measurement setup. The measurement method proposed in this study utilizes closed-loop measurement, with the indicator pointer in rigid contact with the barball. It can be used in outdoor and dusty environments, and is unaffected by light, temperature, and other factors. This study approach improves the robustness of robot calibration. A portable method is crucial for robot calibration, especially when the robot needs to be calibrated at the customer's site. Sending it back to the manufacturer for repairs or borrowing a laser scanner incurs significant time and cost. The method described in this study enables a single individual to perform the calibration during a business trip, 50 effectively solving the challenge of difficult calibrations for customer companies. The measuring tools required for the method proposed in this study weigh less than 8kg. The total weight of the connector and TriCal installed on the robotic arm is under 3 kg. If the artifact is constructed from 304 stainless steel, its weight will not exceed 3.5 kg. The dimensions of the artifact are 120 mm length, 120 mm width, and 170 mm high, and the connector and TriCal are much smaller. After conducting tests, it has been confirmed that the connector, TriCal, the artifact, and three displacement sensors can all be accommodated within a 40-liter cabin bag.

However, this research has some limitations. Such as, significant data fluctuations limited the effectiveness of the EKF algorithm, the Levenberg-Marquardt (LM) algorithm tended to overfit after the fifth iteration, and the artifact was limited to only seven planes, restricting the measurement scope. The future research could consider these issues.

V. Conclusions

This study has introduced a novel calibration setup incorporating a TriCal system and a geometrically adaptable artifact. By integrating the LS algorithm with EKF and LM algorithm with EKF, this research refine the accuracy of the calibration process. It was found that the combined LS with EKF algorithm and LM with EKF notably improved the root mean square error (RMSE) and mean error metrics, thereby enhancing the reliability of robot calibrations under variable operational conditions. Specifically, increasing the number of calibration planes from 4 to 7 improved accuracy by 10%, and reducing the number of measurement points from 175 to 91 increased efficiency by 47.7%, albeit with a minimal accuracy reduction of 2.03%. Although the proposed system is cheap, potable and flexible, there are some limitations require future development. Such as, significant data fluctuations limited the effectiveness of the EKF algorithm, the LM algorithm tended to overfit after the fifth iteration, and the artifact was limited to only seven planes, restricting the measurement scope.

Future research should explore calibration methods that are specifically tailored for harsh or unpredictable environments, such as underwater, or space operations, as this could significantly enhance the robustness and applicability of robotic systems in these fields.

References

[1] Ikenna Enebuse, M. Foo, B. Salam, H. Ahmed, Fhon Supmak, and Odongo Steven Eyobu, "A Comparative Review of Hand-Eye Calibration Techniques for Vision Guided Robots," vol. 9, pp. 113143–113155, Aug. 2021, doi: https://doi.org/10.1109/access.2021.3104514.

[2] H. M. Balanji, A. E. Turgut, and L. T. Tunc, "A novel vision-based calibration framework for industrial robotic manipulators," *Robotics and Computer-Integrated Manufacturing*, vol. 73, p. 102248, Feb. 2022, doi: https://doi.org/10.1016/j.rcim.2021.102248.

[3] W. Yang, S. Li, Z. Li, and X. Luo, "Highly Accurate Manipulator Calibration via Extended Kalman Filter-Incorporated Residual Neural Network," *IEEE Transactions on Industrial Informatics*, vol. 19, no. 11, pp. 10831–10841, Nov. 2023, doi: https://doi.org/10.1109/tii.2023.3241614.

[4] Z. Li, S. Li, and X. Luo, "An overview of calibration technology of industrial robots," *IEEE/CAA Journal of Automatica Sinica*, vol. 8, no. 1, pp. 23–36, Jan. 2021, doi: https://doi.org/10.1109/jas.2020.1003381.

[5] Z. Wang *et al.*, "Field Calibration Method for Industrial Robots Based on Single Position Sensitive Device," *IEEE Transactions on Instrumentation and Measurement*, vol. 72, pp. 1–12, Jan. 2023, doi: https://doi.org/10.1109/tim.2023.3291734.

[6] C. Icli, O. Stepanenko, and I. Bonev, "New Method and Portable Measurement Device for the Calibration of Industrial Robots," *Sensors*, vol. 20, no. 20, p. 5919, Oct. 2020, doi: https://doi.org/10.3390/s20205919.

[7] Z. Li, S. Li, and X. Luo, "Efficient Industrial Robot Calibration via a Novel Unscented Kalman Filter-Incorporated Variable Step-Size Levenberg–Marquardt Algorithm," *IEEE transactions on instrumentation and measurement*, vol. 72, pp. 1–12, Jan. 2023, doi: https://doi.org/10.1109/tim.2023.3265744.

[8] N. A. Nadeau, I. A. Bonev, and A. Joubair, "Impedance Control Self-Calibration of a Collaborative Robot Using Kinematic Coupling," *Robotics*, vol. 8, no. 2, p. 33, Apr. 2019, doi: https://doi.org/10.3390/robotics8020033.

[9] Z. Li, S. Li, O. O. Bamasag, A. Alhothali, and X. Luo, "Diversified Regularization Enhanced Training for Effective Manipulator Calibration," *IEEE Transactions on Neural Networks and Learning Systems*, pp. 1–13, 2022, doi: https://doi.org/10.1109/TNNLS.2022.3153039.

[10] Y. Gan, J. Duan, and X. Dai, "A calibration method of robot kinematic parameters by drawstring displacement sensor," *International Journal of Advanced Robotic Systems*, vol. 16, no. 5, p. 172988141988307, Sep. 2019, doi: https://doi.org/10.1177/17298814198830